

# Tuning Frictional Properties of Kirigami Altered Graphene Sheets using Molecular Dynamics and Machine Learning

*Designing a Negative Friction Coefficient*

Mikkel Metzsch Jensen



Thesis submitted for the degree of  
Master in Computational Science: Materials Science  
60 credits

Department of Physics  
Faculty of mathematics and natural sciences

UNIVERSITY OF OSLO

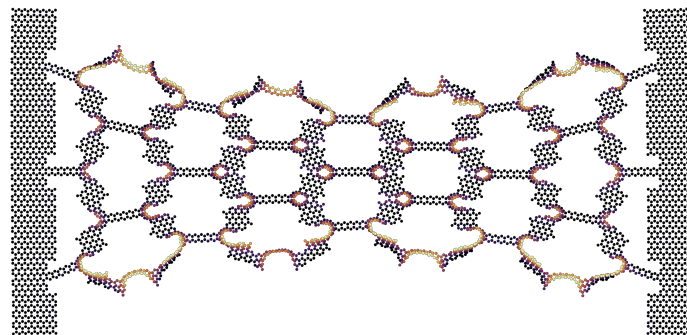
Spring 2023



# Tuning Frictional Properties of Kirigami Altered Graphene Sheets using Molecular Dynamics and Machine Learning

*Designing a Negative Friction Coefficient*

Mikkel Metzsch Jensen





© 2023 Mikkel Metzsch Jensen

Tuning Frictional Properties of Kirigami Altered Graphene Sheets using Molecular Dynamics and Machine Learning

<http://www.duo.uio.no/>

Printed: Reprocentralen, University of Oslo

# Abstract

Abstract.



# Acknowledgments

Acknowledgments.



# List of Symbols

$F_N$  Normal force (normal load)



# Acronyms

**CM** Center of Mass. 14, 15

**MD** Molecular Dynamics. 2, 3, 9, 10, 13

**ML** Machine Learning. 2, 3, 10

**std** Standard Deviation. 16, 17



# Contents

<b>1</b>	<b>Introduction</b>	<b>1</b>
1.1	Motivation . . . . .	1
1.2	Goals . . . . .	3
1.3	Contributions . . . . .	3
1.4	Thesis structure . . . . .	3
<b>I</b>	<b>Background Theory</b>	<b>5</b>
<b>II</b>	<b>Simulations</b>	<b>7</b>
<b>2</b>	<b>Pilot study</b>	<b>9</b>
2.1	Friction simulation parameters . . . . .	9
2.2	Force traces . . . . .	10
2.2.1	Force oscillations . . . . .	10
2.2.2	Decompositions . . . . .	14
2.2.3	Center of mass path . . . . .	14
2.3	Defining metrics for friction . . . . .	16
2.3.1	Kinetic friction . . . . .	16
2.3.2	Static friction . . . . .	17
2.4	Out-of-plane buckling . . . . .	18
2.5	Investigating selected parameters . . . . .	20
2.6	Normal force and stretch dependencies . . . . .	22
2.6.1	Pressure reference for normal load domain . . . . .	23
2.6.2	Contact area . . . . .	23
2.6.3	Stretch . . . . .	24
2.6.4	Normal force . . . . .	26
2.7	Computational cost . . . . .	27
<b>Appendices</b>		<b>29</b>
<b>Appendix A</b>		<b>31</b>
A.1	Sheet stretch . . . . .	31
<b>Appendix B</b>		<b>35</b>
<b>Appendix C</b>		<b>37</b>



# Chapter 1

## Introduction

**Structure of Motivation section:**

1. Introduce and motivate friction broadly.
2. Motives for friction control using a grasping robot as example.
3. Analog to gecko feet where adhesive properties are turned on and off.
4. Interest in origin of friction through nanoscale studies which further motivates the use of MD.
5. Intro to metamaterials and the use of kirigami designs,
6. How to optimize kirigami designs with reference to Hanakata and motivating the use of ML.
7. Out-of-plane buckling motivates the use of kirigami for frictional properties.

Does some of the latter paragraphs belong to the approach section?

### 1.1 Motivation

Friction is a fundamental force that takes part in most of all interactions with physical matter. Even though the everyday person might not be familiar with the term *friction* we recognize it as the inherent resistance to sliding motion. Some surfaces appear slippery and some rough, and we know intuitively that sliding down a snow covered hill is much more exciting than its grassy counterpart. Without friction, it would not be possible to walk across a flat surface, lean against the wall without falling over or secure an object by the use of nails or screws [p. 5] [1]. It is probably safe to say that the concept of friction is integrated in our everyday life to such an extent that most people take it for granted. However, the efforts to control friction dates back to the early civilization (3500 B.C.) with the use of the wheel and lubricants to reduce friction in translational motion [2]. Today, friction is considered a part of the wider field *tribology* derived from the Greek word *Tribos* meaning “rubbing” and includes the science of friction, wear and lubrication [2]. The most compelling motivation to study tribology is ultimately to gain full control of friction and wear for various technical applications. Especially, reducing friction is of great interest as this has tremendous advantages for energy efficiency. It has been reported that tribological problems have a significant potential for economic and environmental improvements [3]:

“On global scale, these savings would amount to 1.4% of the GDP annually and 8.7% of the total energy consumption in the long term.” [4].

On the other hand, the reduction of friction is not the only sensible application for tribological studies. Controlling frictional properties, besides minimization, might be of interest in the development of a grasping robot where a finetuned object handling is required. While achieving a certain “constant” friction response is readily obtained through appropriate material choices during manufacturing, we are yet to unlock the capabilities to alter friction dynamically on the go. One example from nature inspiring us to think along these lines are the gecko feet. More precisely, the Tokay gecko has received a lot of attention in scientific studies aiming to unravel the underlying

mechanism of its “toggable” adhesion properties. Although geckos are able to produce large adhesive forces, they retain the ability to remove their feet from an attachment surface at will [5]. This makes the gecko able to achieve a high adhesion on the feet when climbing a vertical surface while lifting it for the next step remains relatively effortless. For a grasping robot we might consider an analog frictional concept of a surface material that can change from slippery to rough on demand depending on specific tasks.

In the recent years an increasing amount of interest has gone into the studies of the microscopic origin of friction, due to the increased possibilities in surface preparation and the development of nanoscale experimental methods. Nano-friction is also of great concern for the field of nano-machining where the frictional properties between the tool and the workpiece dictates machining characteristics [3]. With concurrent progress in computational power and development of Molecular Dynamics (MD), numerical investigations serve as an extremely useful tool for getting insight into the nanoscale mechanics associated with friction. This simulation based approach can be considered as a “numerical experiment” enabling us to create and probe a variety of high complexity systems which are still out of reach for modern experimental methods.

In materials science such MD-based numerical studies have been used to explore the concept of so-called *metamaterials* where material compositions are designed meticulously to enhance certain physical properties [6][7][8][9][10][11]. This is often achieved either by intertwining different material types or removing certain regions completely. In recent papers by Hanakata et al. [6](2018) [7](2020) numerical studies have showcased that mechanical properties of a graphene sheet, in this case yield stress and yield strain, can be altered through the introduction of so-called *kirigami* inspired cuts into the sheet. Kirigami is a variation of origami where the paper is cut additionally to being folded. While these methods originate as an art form, aiming to produce various artistic objects, they have proven to be applicable in a wide range of fields such as optics, physics, biology, chemistry and engineering [12]. Various forms of stimuli enable direct 2D to 3D transformations through folding, bending, and twisting of microstructures. While original human designs have contributed to specific scientific applications in the past, the future of this field is highly driven by the question of how to generate new designs optimized for certain physical properties. However, the complexity of such systems and the associated design space makes for seemingly intractable problems ruling out analytic solutions.

Earlier architecture design approaches such as bioinspiration, looking at gecko feet for instance, and Edisonian, based on trial and error, generally rely on prior knowledge and an experienced designer [9]. While the Edisonian approach is certainly more feasible through numerical studies than real world experiments, the number of combinations in the design space rather quickly becomes too large for a systematic search, even when considering the simulation time on modern day hardware. However, this computational time constraint can be relaxed by the use of machine learning (ML) which have proven successful in the establishment of a mapping from the design space to physical properties of interest. This gives rise to two new styles of design approaches: One, by utilizing the prediction from a trained network we can skip the MD simulations all together resulting in an *accelerated search* of designs. This can be further improved by guiding the search accordingly to the most promising candidates, as for instance done with the *genetic algorithm* which suggest new designs based on mutation and crossing of the best candidates so far. Another, even more sophisticated approach, is through generative methods such as *Generative Adversarial Networks* (GAN). By working with a so-called *encoder-decoder* network structure, one can build a model that reverses the prediction process. That is, the model predicts a design from a set of physical target properties. In the papers by Hanakata et al. both the *accelerated search* and the *inverse design* approach was proven successful to create novel metamaterial kirigami designs with the graphene sheet.

Hanakata et al. attributes the variety in yield properties to the non-linear effects arising from the out-of-plane buckling of the sheet. Since it is generally accepted that the surface roughness is of great importance for frictional properties it can be hypothesized that the kirigami cut and stretch procedure can also be exploited for the design of frictional metamaterials. For certain designs we might hope to find a relationship between stretching of the sheet and frictional properties. If significant, this could give rise to a variability of the friction response beyond manufacturing material choice. For instance, the grasping robot might apply such a material as artificial skin for which stretching or relaxing of the surface could result in a changeable friction strength; Slippery and smooth when in contact with people and rough and firmly gripping when moving heavy objects. In addition, a possible coupling between stretch and the normal load through a nanomachine design would allow for an altered friction coefficient. This invites the idea of non-linear friction coefficients which might in theory also take on negative values given the right response from stretching. The latter would constitute an extremely rare property. This has (**only?**) been reported indirectly for bulk graphite by Deng et al. [13] where the friction kept increasing during the unloading phase. **Check for other cases and what I can really say here.**

To the best of our knowledge, kirigami has not yet been implemented to alter the frictional properties of a nanoscale system. In a recent paper by Liefferink et al. [14](2021) it is reported that macroscale kirigami can be used to dynamically control the macroscale roughness of a surface through stretching which was used to change the frictional coefficient by more than one order of magnitude. This supports the idea that kirigami designs can in fact be used to alter friction, but we believe that taking this concept to the nanoscale regime would involve a different set of underlying mechanisms and thus contribute to new insight in this field.

## 1.2 Goals

In this thesis we investigate the possibility to alter and control the frictional properties of a graphene sheet through application of kirigami inspired cuts and stretching of the sheet. With the use of MD simulations we evaluate the friction properties under different physical conditions in order to get insight into the prospects of this field. By evaluating variations of two kirigami inspired patterns and a series of random walk generated patterns we create a dataset containing information of the frictional properties associated with each design under different load and stretch conditions. We apply ML to the dataset and use an accelerated search approach to optimize for different properties of interest. The subtask of the thesis are presented more comprehensively in the following.

1. Define a sheet indexing that allows for a unique mapping of patterns between a hexagonal graphene lattice representation to a matrix representation suited for numerical analysis.
2. Design a MD simulation procedure to evaluate the frictional properties of a given graphene sheet under specified physical conditions such as load, stretch, temperature etc.
3. Find and implement suitable kirigami patterns which exhibit out-of-plane buckling under tensile load. This includes the creation of a framework for creating variations within each pattern class. Additionally create a procedure for generating different styles of random walk patterns.
4. Perform a pilot study of a representative subset of patterns in order to determine appropriate simulation parameters to use for the further study along with an analysis of the frictional properties shown in the subset.
5. Create a dataset consisting of the chosen kirigami variations and random walk patterns and analyse data trends.
6. Train a neural network to map from the design space to physical properties such as mean friction, maximum friction, contact area etc. and evaluate the performance.
7. Perform an accelerated search optimizing for interesting frictional properties using the ML model. This should be done both through the pattern generation procedures and by following a genetic algorithm approach.
8. Use the most promising candidates from the accelerated search to investigate the prospects of creating a nanomachine setup which exhibits a negative friction coefficient.
9. Study certain designs of interest with the scope of revealing underlying mechanism. This includes simple correlation analysis but also a visualization of feature and gradient maps of the ML network.

Is the list of subtask too specific? Some of the details here might be better suited for the thesis structure section.

## 1.3 Contributions

What did I actually achieve

## 1.4 Thesis structure

How is the thesis structured.



# Part I

# Background Theory



## **Part II**

# **Simulations**



# Chapter 2

## Pilot study

Having defined our system, we carry out an initial study of the numerical approach. This includes an analysis of how to define and measure the frictional properties of interest, and an investigation of the main parameters governing the numerical solutions. From this point of view we decide on suitable parameters for the remaining study. Particularly, we investigate the frictional behaviour under the variation of load and stretch for a selected set of configurations which serves as a baseline for later comparison and an assessment of the prospects of Kirigami modifications for friction.

### 2.1 Friction simulation parameters

The MD simulation is governed by a small set of parameters, some which are related directly to the numerical aspects of the simulation and other related to the physical conditions we are simulating. Thus, we differentiate between the two main categories: 1) *Physical*, parameters which alter the physical conditions of the “numerical experiment” and are expected to effect the frictional behaviour. 2) *Numerical*, parameters which are related more closely to the numerical procedure itself, expected to influence the simulation dynamics, which should be chosen to ensure the most stable results. For the purpose of creating the machine learning dataset most of these parameters will be kept constant with only a subset of the physical parameters being varied. The parameters are summarized in Table 2.1 where the grey shaded area marks the parameters, Configuration, stretch and load, which we will vary for the dataset. Due to the great number of parameters it is unreasonable to make an exhaustive search of all parameters before deciding on the final settings. Instead, we take a basis in the parameters used in similar studies **SOURCES** and adjust them as we carry out the initial analysis of the simulation results. Thus, we start at values most representative for other similar simulations and adjust according to the stability of the results and the computation time. Since we are going to introduce a lot of complexity to the system, through the cut and stretch deformation, we are less concerned about aligning parameters for comparison. Instead of presenting the process of narrowing down the final parameters in a chronological manner, we have shown the final choice shown in Table 2.1 which we will discuss throughout the following presentation of the pilot study. Notice, that the values in Table 2.1 serve as default values which are used when nothing else is stated.

**Table 2.1:** Parameters of the numerical MD simulation for measuring friction. The values correspond to the final choice used for the dataset. The shaded area denote the parameters varied in the ML dataset.

Category	Parameter	Value	Description
Physical	$T$	300 K	Temperature.
	$v_{\text{slide}}$	20 m/s	Sliding speed for the sheet translation.
	$K$	inf	Spring constant for the coupling between the virtual atom and the sheet pull blocks.
	Scan direction	$(x, y) = (0, 1)$ (zigzag direction)	The direction for which we translate the sheet.
	Sheet configuration	Contiguous	Binary mapping describing which atoms are removed (0) and which is still present (1) in the graphene sheet.
	Stretch amount	0% - rupture	The relative stretch of the sheet.
	$F_N$	[0.1, 10] nN	Applied normal force to the pull blocks.
Numerical	$dt$	1 fs	Integration timestep.
	$t_R$	15 ps	Relaxtion time before strething.
	Pauses	5 ps	Relaxtion pauses after stretch, and during the normal load phase (before translating the sheet).
	Stretch Speed	$0.01 \text{ ps}^{-1}$	The rate of stretching for the sheet.
	Slide distance	400 Å	How far to translate the sheet.
	Sheet size	$130.029 \times 163.219 \text{ \AA}$	Spatial 2D size of the sheet.
	Pull block size	$2 \times 130.029 \times 15.183 \text{ \AA}$	Spatial 2D size of the pull blocks.

## 2.2 Force traces

We begin by assessing the friction force traces, i.e. force vs. time curves, for a single friction simulation using the default parameters shown in ?? for a non-cut sheet with no stretch applied and a normal load of 1 nN.

### 2.2.1 Force oscillations

We evaluate the friction force as the force acting on the sheet from the substrate. We consider initially the force component  $F_{\parallel}$  parallel to the drag direction as plotted in Fig. 2.1. We use a sample rate of  $10 \text{ ps}^{-1} = 100 \text{ timesteps}^{-1}$  for which each sample is the mean value of the preceding 100 timesteps. We observe immediately that the data carriers oscillations on different time scales matching our general expectations for sliding involving periodic surfaces. By applying a savgol filter to the data with a polyorder of 5 and window length of 150 timesteps (corresponding to a sliding distance of 3 Å or a time window of 15 ps) we can qualitatively point out at least two different frequencies of oscillation. During the first 10 Å of sliding, seen in Fig. 2.1a, we see roughly three waves on the savgol filter corresponding to a relative high frequency, while for the duration of 100 Å of sliding, seen in Fig. 2.1b, the same savgol filter reveals a lower frequency on top, creating the visual pattern of a wavepacket. The data does not indicate clear signs of stick-slip behaviour as otherwise found in other studies, e.g. by Zhu and Li [15] for graphene on gold, who saw a more typical saw tooth shape in the force trace. Beside the difference in substrate material, using gold instead of silicon, they used a lower sliding speed of 10 m/s and a soft spring of  $K = 10 \text{ N/m}$ . By adopting those parameters we get a slightly different force trace behaviour as shown in Fig. 2.1c and Fig. 2.1d. This change breaks the symmetry in the force oscillations, but still does not produce any significant discontinuities in the trace. By keeping the spring constant  $K = 10 \text{ N/m}$  and lowering the sliding speed further down to 1 m/s we are able to demonstrate a proper stick-slip behaviour as shown in Fig. 2.1e and Fig. 2.1f. Considering all three simulations we might classify the results from the default settings,  $K = \text{inf}$ ,  $v = 20 \text{ m/s}$ , as smooth sliding,  $K = 10 \text{ N/m}$ ,  $v = 10 \text{ m/s}$ , as a transition phase with possible occasional slipping, and  $K = 10 \text{ N/m}$ ,  $v = 1 \text{ m/s}$  as certain stick-slip behaviour.

Refer a bit to theory on this one

However, the low sliding speed comes with a high computational cost which is the reason that we choose a sliding speed of 20 m/s. The choice of an infinite spring constant is related to the stability of the measurements as discussed later [make reference](#).

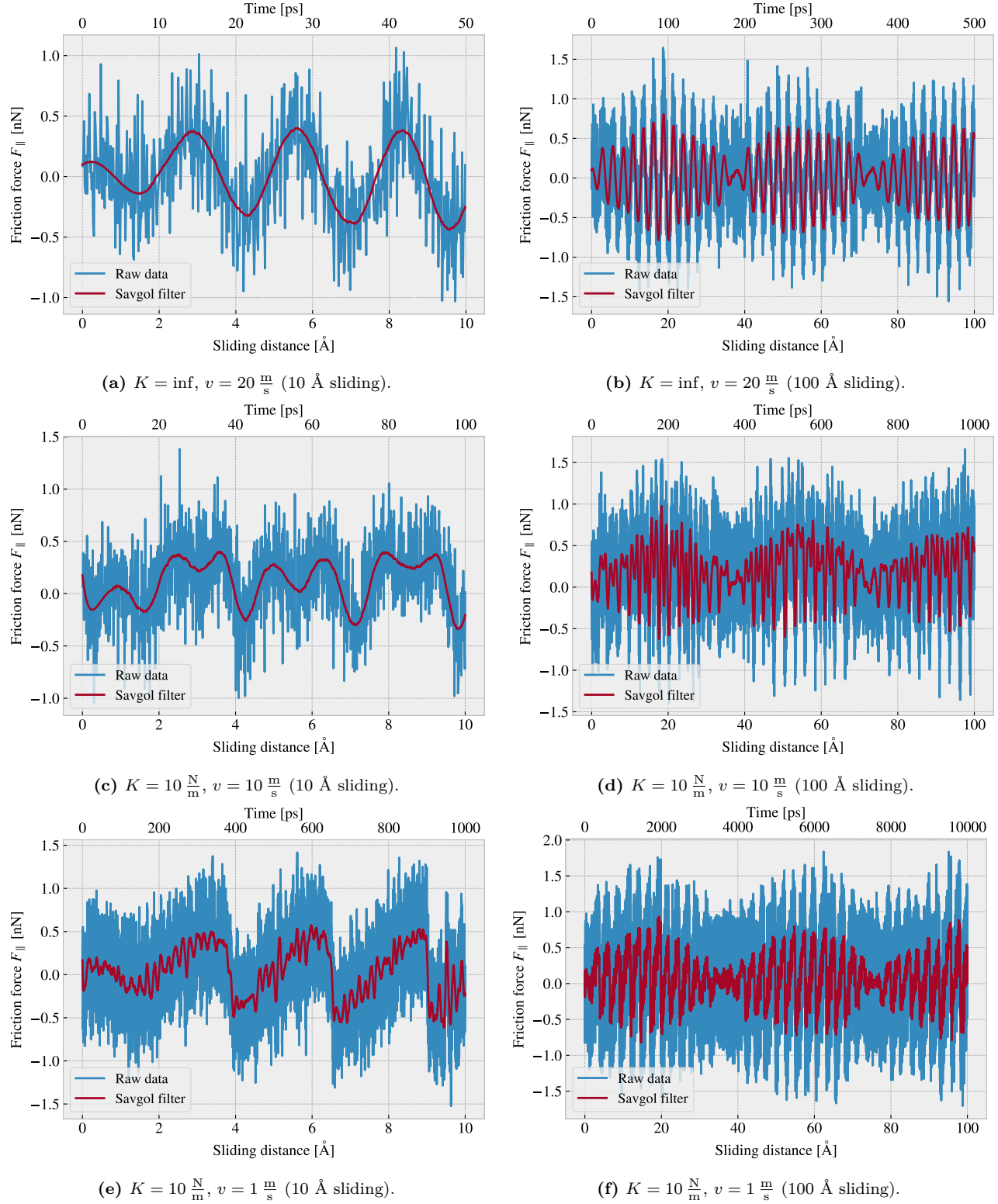


**Figure 2.1:** Force traces of the friction force  $F_{\parallel}$  with respect to the drag direction between acting from the substrate on the full sheet and substrate. The force traces is plotted against the sliding distance (lower x-axis) and the corresponding sliding time (upper x-axis). The sliding distance is measured by displacement of the virtual atom tethering the sheet. The red line represents a savgol filter with window polyorder 5 and window length of 150 timesteps (corresponding to a sliding distance of 3  $\text{\AA}$  or a time window of 15 ps). Each row, (a,b), (c,d), (e,f), represents a different choice of the spring constant  $K$  and sliding speed  $v$ , while the columns show the same result for two different time scales. The default settings are represented in figure (a) and (b).

By performing a Fourier Transform on the data, using the default parameters, we can quantify the leading frequencies observed in figure Fig. 2.1a and Fig. 2.1b. The Fourier transform is shown in Fig. 2.2a, and by plotting the two most dominant frequencies  $f_1 = 0.0074 \text{ ps}^{-1}$  and  $f_2 = 0.0079 \text{ ps}^{-1}$  as a sine sum,  $\sin(2\pi f_1) + \sin(2\pi f_2)$ , we find a qualitatively convincing fit to the observed wavepacket shape as seen in Fig. 2.2b. We can convert the frequencies according to that of a wavepacket. By using the trigonometric identity

$$\begin{aligned}\sin(a+b) &= \sin(a)\cos(b) + \cos(a)\sin(b), \\ \sin(a-b) &= \sin(a)\cos(b) - \cos(a)\sin(b),\end{aligned}$$

and decomposing the frequencies as  $f_1 = a - b$ ,  $f_2 = a + b$ , we can rewrite the sine sum as the sinusoidal product

$$\begin{aligned}\sin(2\pi f_1) + \sin(2\pi f_2) &= \sin(2\pi(a-b)) + \sin(2\pi(a+b)) \\ &= \sin(2\pi a)\cos(2\pi b) + \cancel{\cos(2\pi a)\sin(2\pi b)} + \sin(2\pi a)\cos(2\pi b) - \cancel{\cos(2\pi a)\sin(2\pi b)} \\ &= 2\sin(2\pi a)\cos(2\pi b),\end{aligned}$$

with

$$\begin{aligned}a &= \frac{f_1 + f_2}{2} = 0.0763 \pm 0.0005 \text{ ps}^{-1}, & b &= \frac{f_2 - f_1}{2} = 0.0028 \pm 0.0005 \text{ ps}^{-1}, \\ &= 0.381 \pm 0.003 \text{ \AA}^{-1}, & &= 0.014 \pm 0.003 \text{ \AA}^{-1},\end{aligned}$$

where the latter frequency is denoted with respect to the sliding distance. This makes us recognize the high oscillation frequency as  $a$  and the low frequency as  $b$ . The faster one has a period of  $T_a = 2.62 \pm 0.02 \text{ \AA}^1$  which corresponds well with the magnitude of the lattice spacing and especially that of graphene at  $2.46 \text{ \AA}$  as expected theoretically. The longer period  $T_b = 71 \pm 15 \text{ \AA}^{-1}$  is not obviously explained. We noticed a similar long period oscillation for all three cases, Fig. 2.1b, Fig. 2.1d and Fig. 2.1f, regarding stick-slip behaviour, and thus we do not believe that this is directly related. The initial build up in friction force is reminiscent of a friction strengthening, which is often reported SOURCE, but the periodicity goes against this idea. Instead, we might attribute it to some kind of phonon resonance which could be a physical phenomenon or simply a feature of our MD modelling.

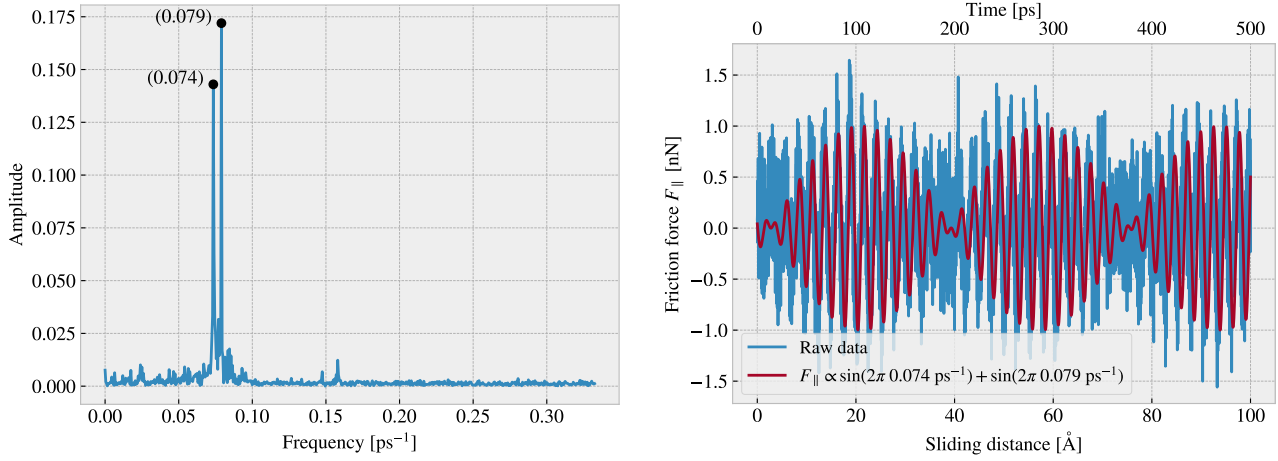


**Figure 2.2:** Fourier transform analysis of the full friction force data (all  $400 \text{ \AA}$  sliding distance) shown in Fig. 2.1. (a) shows the two most dominant frequency peaks. Note that no significant peaks were found in a higher frequency than included here. (b) shows a comparison between the raw data and the wavefunction corresponding to the two peaks in figure (a).

<sup>1</sup>The uncertainty  $\Delta y$  is calculated as  $\Delta y = \left| \frac{\partial y}{\partial x} \Delta x \right|$  for uncertainty  $\Delta x$  and  $y(x)$

## 2.2.2 Decompositions

In the previous analysis we have looked only at the friction force for the full sheet, including the rigid pull blocks, and with respect to the drag direction. We found this way of measuring the friction force to be the most intuitive and reliable, but we will present the underlying arguments for this choice in the following.

Due to the fact that we are only applying cuts to the inner sheet, and not the pull blocks, it might seem more natural to only consider the friction on that part. If the desired frictional properties can be achieved by altering the inner sheet one can argue that any opposing effects from the pull blocks can be mitigated by simply scaling the relative size between the inner sheet and the pull blocks. However, when looking at the force traces decomposed with respect to the inner sheet and pull block regions respectively, see Fig. 2.3a, we observe that the friction force arising from those parts are seemingly antisymmetric. That is, the distribution of the frictional pull from the substrate on the sheet is oscillating between the inner sheet and the pull block. Keeping in mind that normal force is only applied to the pull blocks we might take this as an intrinsic feature of the system which does not necessarily disappear by scaling of the spatial ratio between the inner sheet and pull block. Any interesting friction properties might depend on this internal distribution of forces. Hence, we hedge our bets and use the full sheet friction force as a holistic approach to avoid excluding relevant information in the measurement data.

Similar we might question the decision of only considering the frictional force projected onto the sliding direction as we are then neglecting the “side shift” induced during sliding. In Fig. 2.3b we show the decomposition in terms of force components parallel  $F_{\parallel}$  and perpendicular  $F_{\perp}$  to the sliding direction respectively. We notice that the most dominant trend appears for the parallel component. If we want to include the perpendicular component as well we would have to evaluate friction as the length of the force vector instead, but this would remove the sign of the force direction and shift the mean friction force up as we clearly see both negative and positive contributions in the parallel force trace. One option to accommodate this issue is by using the vector length for the magnitude but keeping the sign from the parallel component. However, we omit such compromises as this might make the measurement interpretation unnecessary complex, and we use only the parallel component going forward.

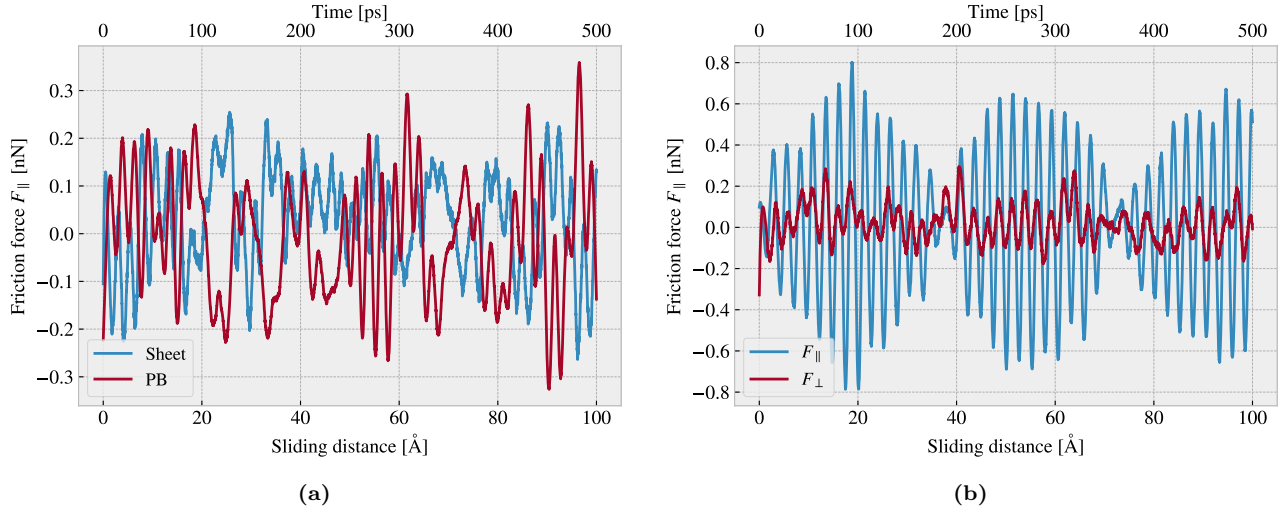


**Figure 2.3:** Friction force decomposition on the default parameter force trace shown in Fig. 2.1 showing only the applied savgol filters. (a) Decomposition into group inner sheet (sheet) and pull blocks (PB). (b) Decomposition into parallel ( $F_{\parallel}$ ) and perpendicular ( $F_{\perp}$ ) to drag sliding direction.

## 2.2.3 Center of mass path

From the previous observations of the force traces Fig. 2.1 we demonstrated both smooth sliding and stick-slip behaviour. Considering the force decomposition in Fig. 2.3b we know that the frictional forces in the perpendicular direction to sliding is also present. By looking at the  $x, y$ -position for the sheet Center of Mass (CM) we see a qualitatively different behaviour when reconsidering the spring constant and sliding speed investigated in Fig. 2.1 which is shown in Fig. 2.4. The default case in Fig. 2.4a shows a rather straight path forward with only a

small side motion in comparison to the cases in Fig. 2.4b and Fig. 2.4c. However, the CM accelerates and deaccelerates with a high frequency, much too high to be associated with the lattice spacing on the order of 2.46 Å (interatomic distance of 1.42 Å). One possible explanation is that the sheet and substrate constitutes an incommensurable contact for which travelling kink excitations make the atoms move in such a way that the sheet CM is incremented in small “burst”. When looking at the  $K = 10 \frac{\text{N}}{\text{m}}$ ,  $v = 10 \frac{\text{m}}{\text{s}}$  case in Fig. 2.4b we see a completely different CM path where the rapid parts aligns visually better with the force oscillations shown earlier in Fig. 2.1d. The CM accelerates forward and the deaccelerates in combination with a side motion that lead to the CM path making a loop as it slows down. Finally we have the  $K = 10 \frac{\text{N}}{\text{m}}$ ,  $v = 1 \frac{\text{m}}{\text{s}}$  in Fig. 2.4b which is confirmed to have stick-slip behaviour in Fig. 2.1f. Here the CM path shows a more chaotic movement between acceleration which also aligns visually well with the timing of the slips seen in Fig. 2.1f. The chaotic motion is not obviously connected to the stick-slip motion, but we omit a further investigation as this is not corresponding to the parameters that we will be using.

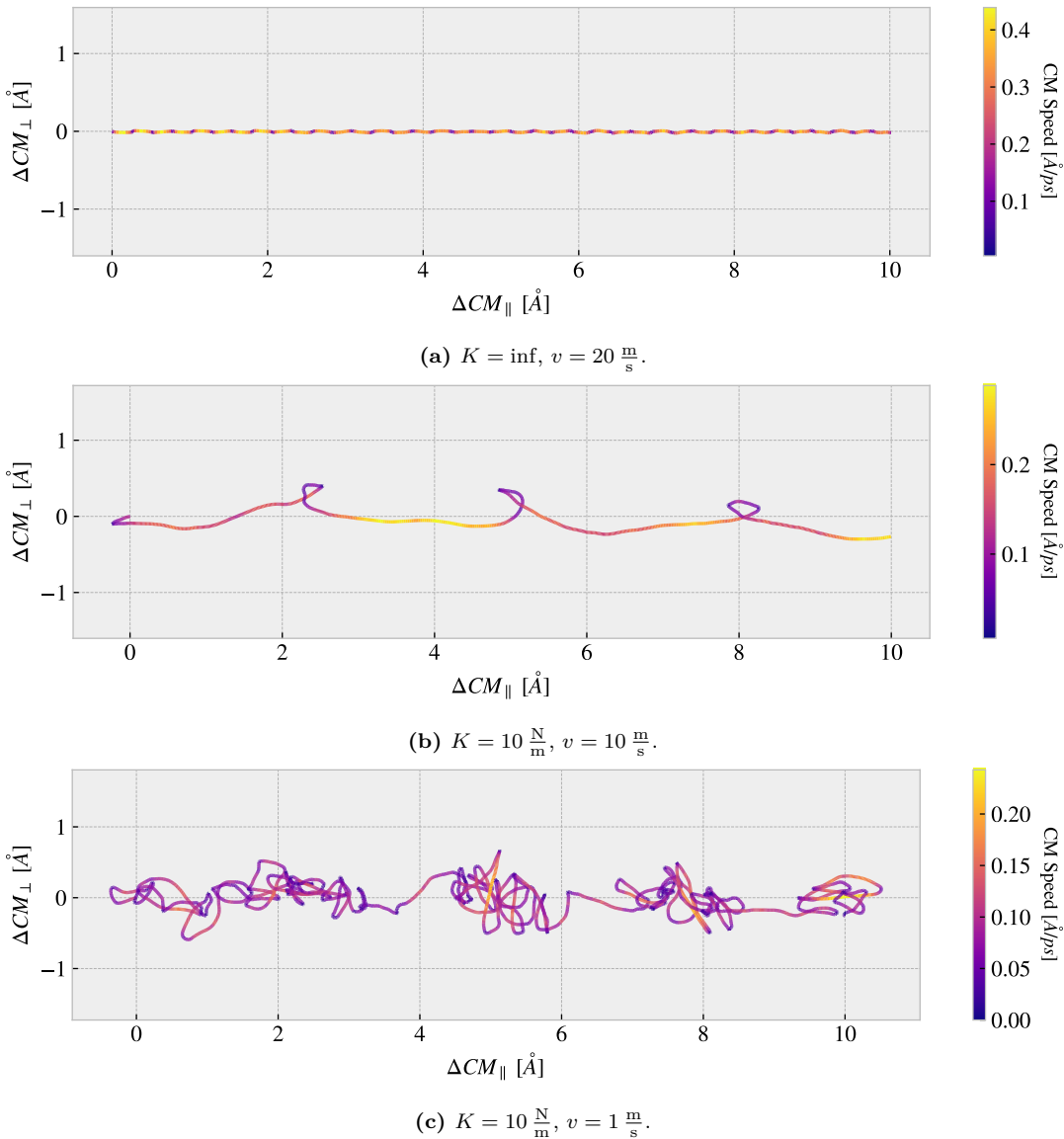


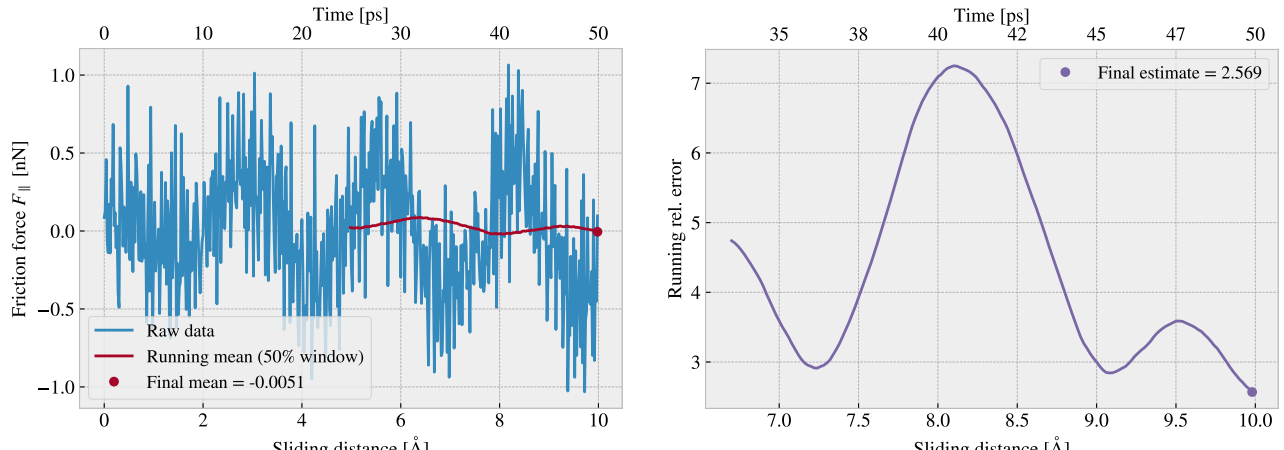
**Figure 2.4:** Center of Mass (CM) position relative to the start of the sliding phase in terms of the direction parallel to the sliding direction  $\Delta COM_{\parallel}$  and the axis perpendicular to the sliding direction  $\Delta COM_{\perp}$ . The colorbar denotes the absolute speed of the CM motion. Figure a-c shows different parameters used for the spring constant  $K$  and sliding speed  $v$  similar to that used in Fig. 2.1. (a) Default:  $K = \infty$ ,  $v = 20 \frac{\text{m}}{\text{s}}$ . (b)  $K = 10 \frac{\text{N}}{\text{m}}$ ,  $v = 10 \frac{\text{m}}{\text{s}}$ . (c)  $K = 10 \frac{\text{N}}{\text{m}}$ ,  $v = 1 \frac{\text{m}}{\text{s}}$

## 2.3 Defining metrics for friction

In order to evaluate the frictional properties of the sheet we aim to reduce the force trace results, addressed in section Sec. 2.2, into single metrics describing the kinetic and static friction respectively.

### 2.3.1 Kinetic friction

We measure kinetic friction as the mean of the friction force trace. More precisely, we take the mean value of the latter half of the dataset in order to ensure that we are sampling from a stable system. For a full sliding simulation of 400 Å we thus base our mean value on the latter 200 Å (1000 ps) of sliding. In Fig. 2.5a we have shown the force trace for the first 10 Å of sliding together with a 50% running mean window. The choice of such a short sliding distance is merely to illustrate the sampling procedure, and we see that the final mean estimate (marked with a dot) takes a negative value due to the specific cut-off of the few oscillations captured here. Nonetheless, one approach to quantify the uncertainty of the final mean estimate is to consider the variation of the running mean preceding the final mean value. The more the running mean fluctuates the more uncertainty associated with the final estimate. Only the running mean “close” to the ending should be considered, since the first part will rely on data from the beginning of the simulation. From the Fourier analyse in section Sec. 2.2.1 we found the longest significant oscillation period to be  $\sim 71 \text{ \AA}^{-1}$  corresponding to  $\sim 35\%$  of the running mean window which gives a window length of 200 Å when including all the data. Hence, we use the standard deviation of the final 35% of the running mean to approximate the uncertainty of the final mean value. We consider the standard deviation (std) as an estimate of the absolute error and calculate the relative error by a division of the final mean value. In Fig. 2.5b we showcase a running relative error based on the std, with a window of length 35% the mean window, in a continuation of the illustrative case of a 10 Å sliding from Fig. 2.5a. In this case we get an extremely high relative error of  $\sim 257\%$ , but this is desirable since the sampling period leads to an unphysical negative value which should be associated with a high uncertainty.



(a) Running mean with window length 5 Å (50% the data length). (b) Running std with window length 1.75 Å (35% the mean window length.)

**Figure 2.5:** Running mean (a) and running relative error (std) (b) on the friction force data from a reduced sliding distance of 10 Å. The running mean window is 50% the data length while the running std window is 35% the running mean window length. The values are plotted at the end of their respective windows such that window precedes the actual point on the graph.

When including the full dataset of 400 Å of sliding, such that the std window actually matches with the longest period of oscillations expected, we get a final relative error of  $\sim 12\%$  as shown in fig Fig. 2.6. This is arguable just at the limit of an acceptable error, but as we shall see later on in Sec. 2.6 this high relative error is mainly associated with the cases of low friction. When investigating different configurations under variation of load and stretch we see a considerable lower relative error as the mean friction evaluates to higher values. One interpretation of this finding is simply that the oscillations in the running mean are to some degree independent of

the magnitude of the friction. In that case, the relative error will spike for the low friction cases, and the absolute error might be there more reliable measure, i.e. taken simple the std without dividing by the final mean value.

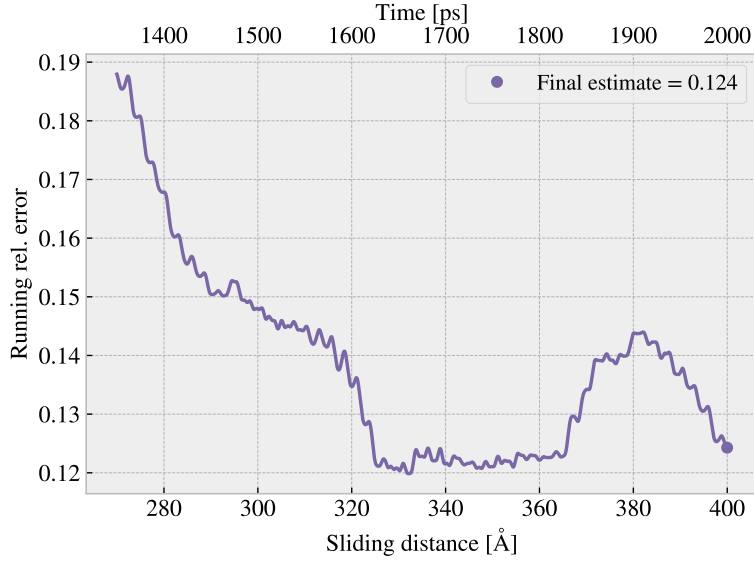


**Figure 2.6:** Running standard deviation (std) for a full 400 Å sliding simulation. The running std window is 70 Å (35% the running mean window of 50% the data length).

### 2.3.2 Static friction

The maximum value is one of the common choices for addressing static friction, even though the definition of static friction is a bit vague. When considering the force traces in Fig. 2.1 we observe that the force oscillations increase in magnitude toward a global peak at  $\sim 20 \text{ \AA}$ . Thus, one could be inclined to identify this peak as the maximum value associated with the static friction force. However, as we have already clarified, this steady increase in friction is a part of a slower oscillation which repeats by a period of  $\sim 71 \text{ \AA}^{-1}$ . By plotting the top three max values recorded during a full 400 Å simulation, for 30 logarithmically spaced load values in the range  $[0.1, 100] \text{ nN}$ , we observe that the global max in fact rarely fall within this first oscillation period as shown in Fig. 2.7. Only 2/30 global maxima and 4/90 top three maxima can be associated to the start of the sliding by this definition. Thus, this result suggests that our default system does not yield a static friction response in the sense of an initial increase in friction due to a depinning of the sheet from the static state **Is this probably defined in the theory section?** Some parameter changes that might increase the likelihood of seeing a significant static friction response is either extending the relaxation period, as static friction is theorized to increase logarithmically with time, or to increase the sliding force more slowly and through a soft spring tethering. As an attempt to test parts of this hypothesis we run a series of simulations with varying spring constant,  $K \in [5, 200] \text{ nN}$  including also  $K = \inf$ , but keeping the relaxation time and sliding speed at the default values. The result is shown in Fig. 2.8. The results do not show any support of the hypothesis that a softening of the spring constant will eventually lead to the maxima occurring in the first period of sliding. We note that this might be suppressed by having a too short relaxation period or a too high sliding speed, related to the rate of which force increased initially, but due to the ambiguousness in the assessment of the static friction we will mainly concern ourselves with the kinetic friction in the remaining of this thesis.

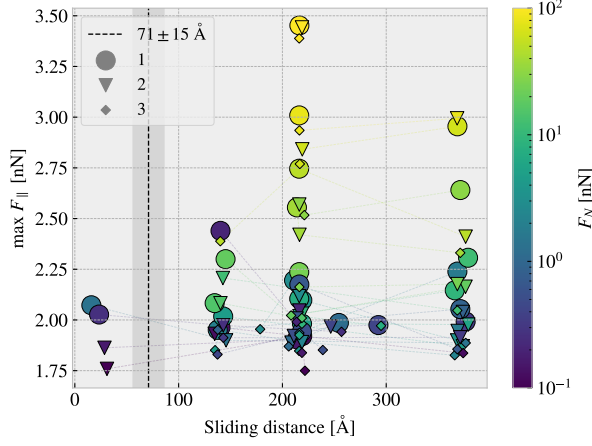


**Figure 2.7:** Distribution of top three max friction force peaks for 30 uniformly sampled normal forces  $F_N \in [0.1, 10]$  nN. The dotted line and the grey area marks the slowest significant oscillation period found in the data and thus marking a dividing line for whether a peak falls within the “beginning” of the sliding simulation.

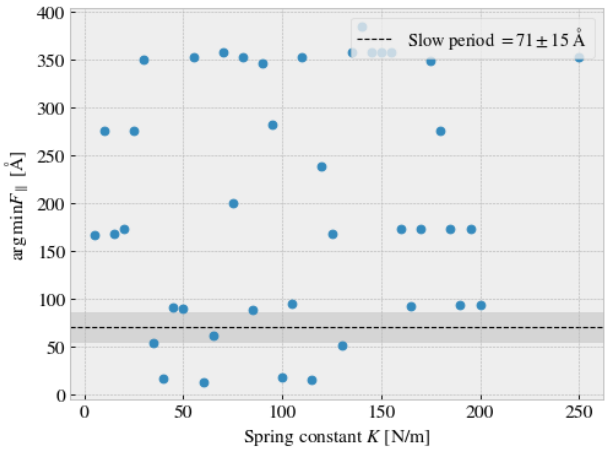


**Figure 2.8:** Sliding displacement for the max friction peak to appear as a function of spring constant. Fixmove is tmp mapped to  $K = 200$  here without any discontinuous lines.

## 2.4 Out-of-plane buckling

The out-of-plane buckling is one of the original motivations for investigating the application of Kirigami cuts in the context of friction properties. Therefor, we perform a stretch simulation, at low temperature ( $T = 5$  K) without any substrate, in order to verify that we are able to reproduce an out-of-plane buckling with the intended patterns described in ???. For this investigation we include the non-cut sheet, the Tetrahedron (7, 5, 1) and the Honeycomb (2, 2, 1, 5) pattern. We quantify the out-of-plane buckling by assessing the distribution of atoms along the z-direction (perpendicular to the plane) during stretching. We calculate the minimum and maximum z-value as well as the atom count quartiles 1%, 10%, 25%, 50% (median), 75%, 90% and 99% as shown in figure Fig. 2.9. The results show significant buckling for the Tetrahedron and Honeycomb patterns in comparison to the non-cut sheet which only exhibit minor buckling of  $\sim 2$  Å which is on the same order as the lattice spacing. Moreover, we notice that the Tetrahedron pattern buckles more in consideration to the min. and max. peaks while the remaining quantiles actually seem to be more closely spaced than for the Honeycomb. By addressing the simulation visually, using the Open Visualization Tool OVITO, we find that this can be attributed to fringes on the edge “flapping around” and thus increasing the min. and max. values.

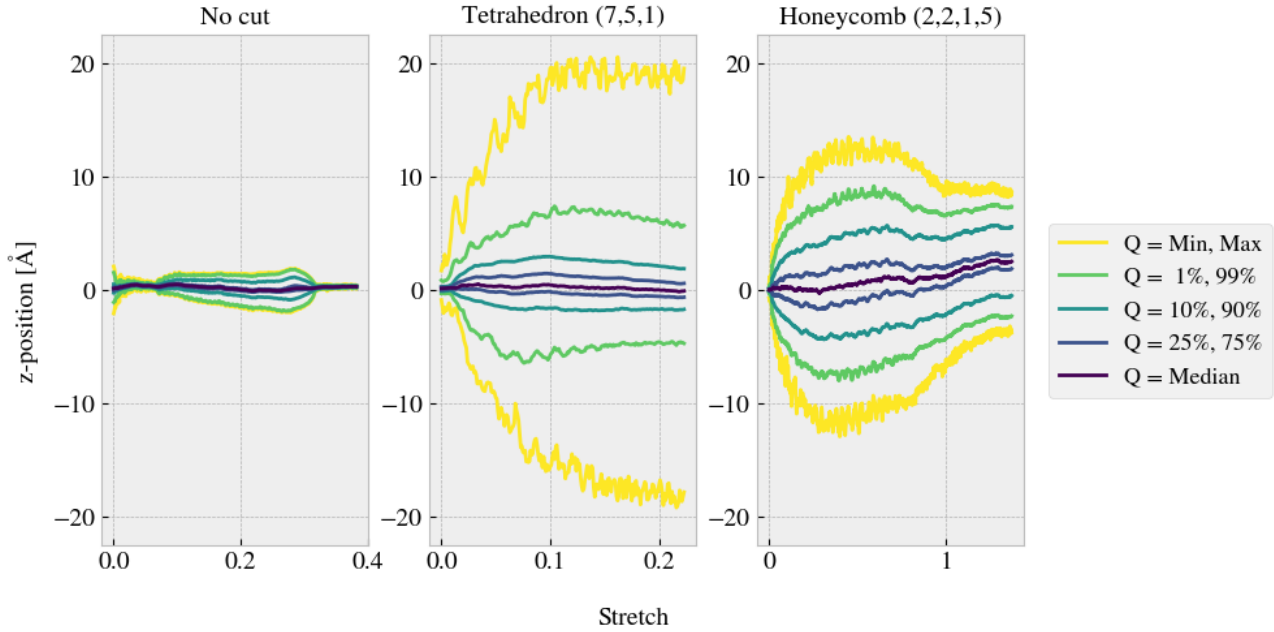


**Figure 2.9:** Out-of-plane buckling during stretching of the No cut, Tetrahedron (7, 5, 1) and Honeycomb (2, 2, 1, 5) sheet respectively in vacuum at low temperature  $T = 5$  K. The buckling is measured by the distribution of the atom z-position (perpendicular to the sheet plane), for which the colors indicates selected quantiles. The yield strain were, reading from left to right, 0.38, 0.22 and 1.37.

Given the confirmation of out-of-plane buckling in a vacuum, as seen in Fig. 2.9, we reintroduce the substrate in order to investigate whether this effect carries over to a change in contact area. We raise the temperature to the default value of  $T = 300$  K. We keep the normal force off and let the sheet stick purely by the adhesion forces between the sheet and substrate. We quantify the contact area through the relative amount of atoms in the sheet within chemical range of the substrate. The cut-off for this interaction is set to 4 Å, inspired by [16], corresponding to  $\sim 120\%$  the LJ equilibrium distance. Usually the contact area is calculated as the number of contacting atoms multiplied with an associated area for each atom. However, since we are not interested in the absolute value of the actual area, but rather the relative change, we omit the multiplication factor. That is, we consider the relative number of atoms within contact range, which is proportional to the contact area, as our metric of choice. The relative contact for the three configurations (No cut, Tetrahedron (7, 5, 1) and Honeycomb (2, 2, 1, 5)) during stretching are shown in figure Fig. 2.10. The figure reveals a significant drop in contact as the sheets are stretched, which agrees qualitatively with the buckling observed without the substrate (Fig. 2.9). The Honeycomb pattern turns out to be both the most stretchable, with a rupture strain at 127% its original length, and the one with the biggest decrease in relative contact down to approximately 43%. Notice, that the relative contact is never actual 1.0 but instead maxes out at around 96% with no stretching. This is attributed to the temperature fluctuations and the choice of cut-off.

Selected frames from the simulation result are shown in appendix Appendix A.1 which reveals a bit more information of how the buckling occurs. The Tetrahedron pattern deforms rather quickly and smoothly into small tetrahedron spikes, as the name suggests. While the Tetrahedron deformation appeared rather uniformly the Honeycomb pattern deforms initially from one side first. As the sheet stretches more rows of the pattern are activated, producing the honeycomb looking shape when seen from above. As both patterns approach the rupture point the tensions lead to a small increase in the relative contact again. This agrees with the results in Fig. 2.9 where the buckling reduces slightly towards the end.

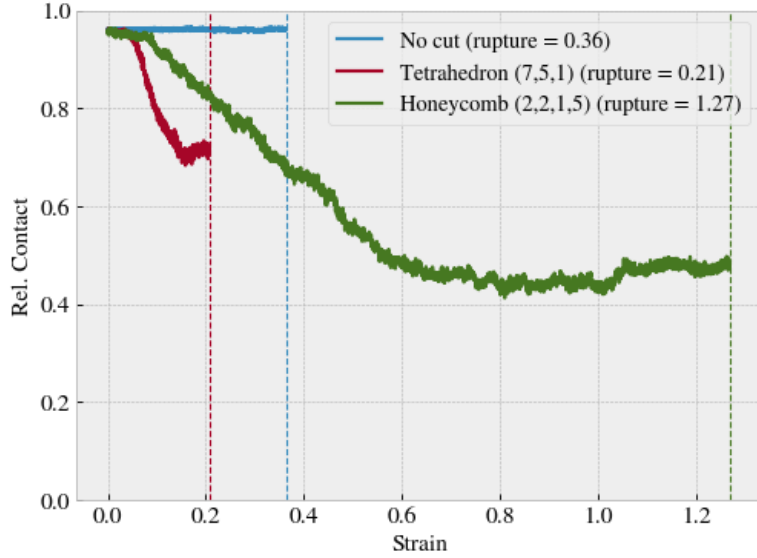


**Figure 2.10:** Relative contact, given as the relative number of atom in the sheet being within chemical interaction range, vs. strain of the sheet. The cut-off for the interaction range is 4 Å corresponding to  $\sim 120\%$  the LJ equilibrium distance. No normal force is applied and temperature is kept at  $T = 300$  K.

Compare figure Fig. 2.10 to that of figure Fig. 2.15 where multiple simulations constitute the stretch-contact curve.

## 2.5 Investigating selected parameters

We investigate the importance of the physical variables  $T$ ,  $v_{\text{slide}}$  and  $K$  (make plots for scan angle as well?) and the choice of timestep  $dt$ . This is done partly understand how the dependencies relate to theoretical, numerical and experimental results, and partly to understand how these parameter choices defines the regime for our multi configurational search. We use the default parameters in ?? with exception of the single parameter of interest which is varied in a reasonable range of the default choice. In Fig. 2.11–Fig. 2.14 the kinetic friction estimate and the max friction force is shown as a function of  $T$ ,  $v_{\text{slide}}$ ,  $K$  and  $dt$  respectively. For the kinetic friction estimate the absolute error is denoted by a shaded error which linearly connects the points.

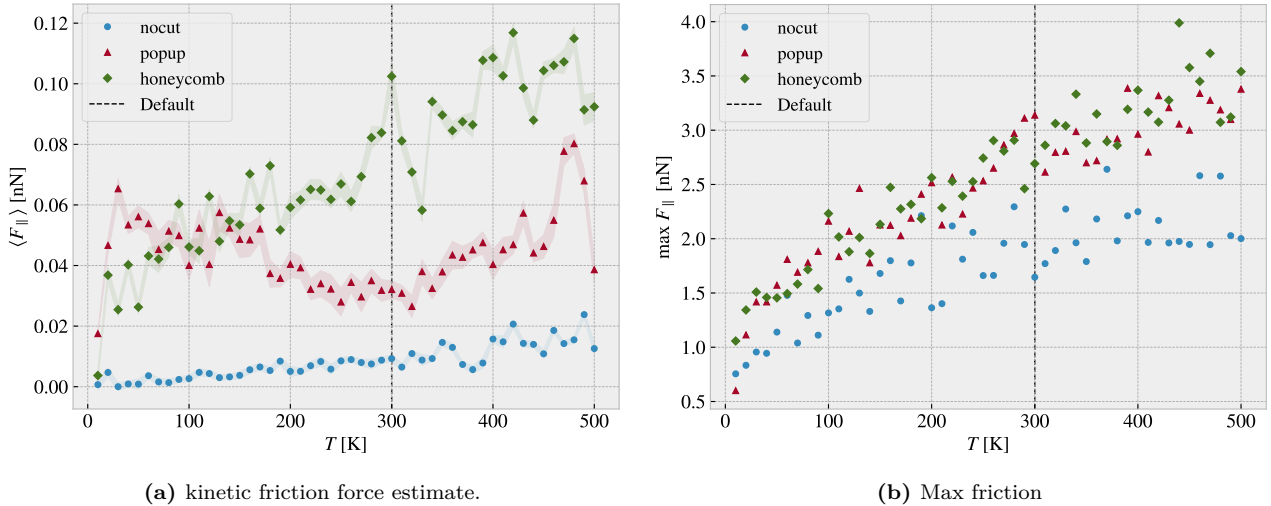


**Figure 2.11:** Temperature.

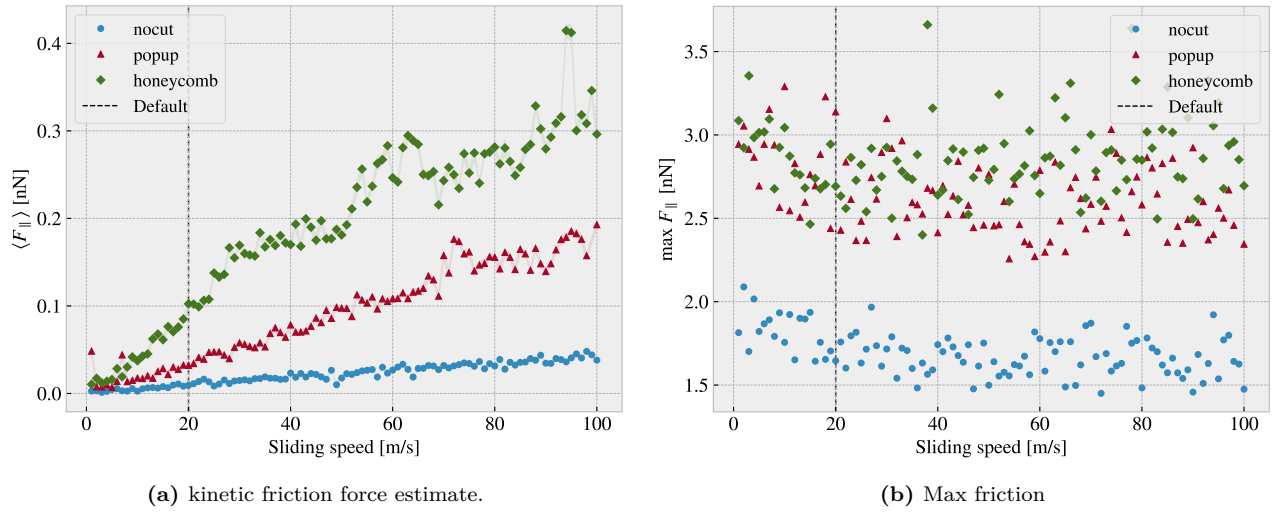


Figure 2.12: Sliding speed

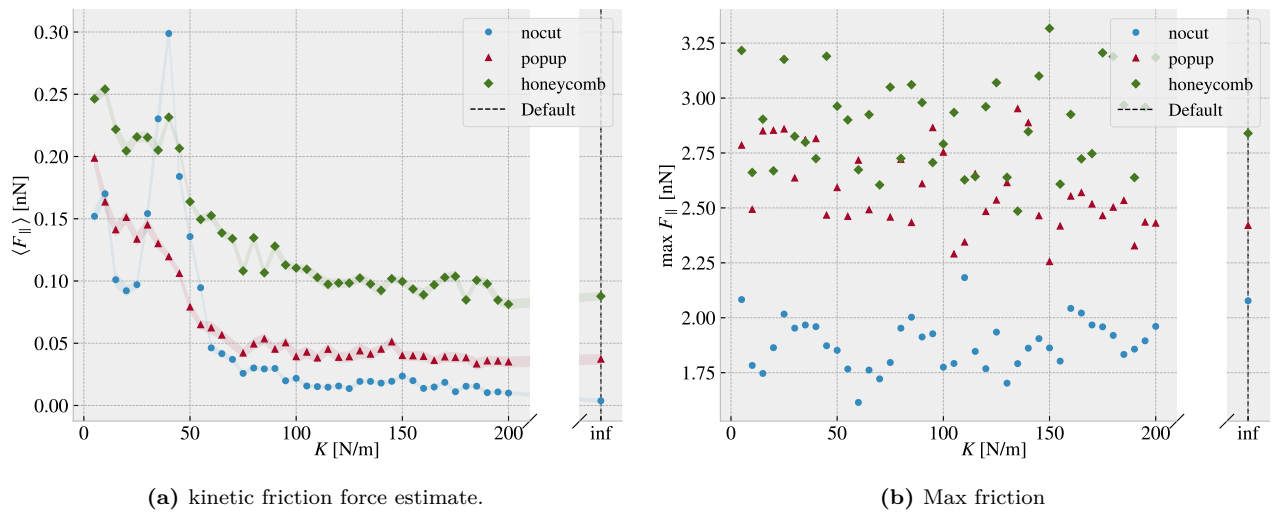


Figure 2.13: Spring constant

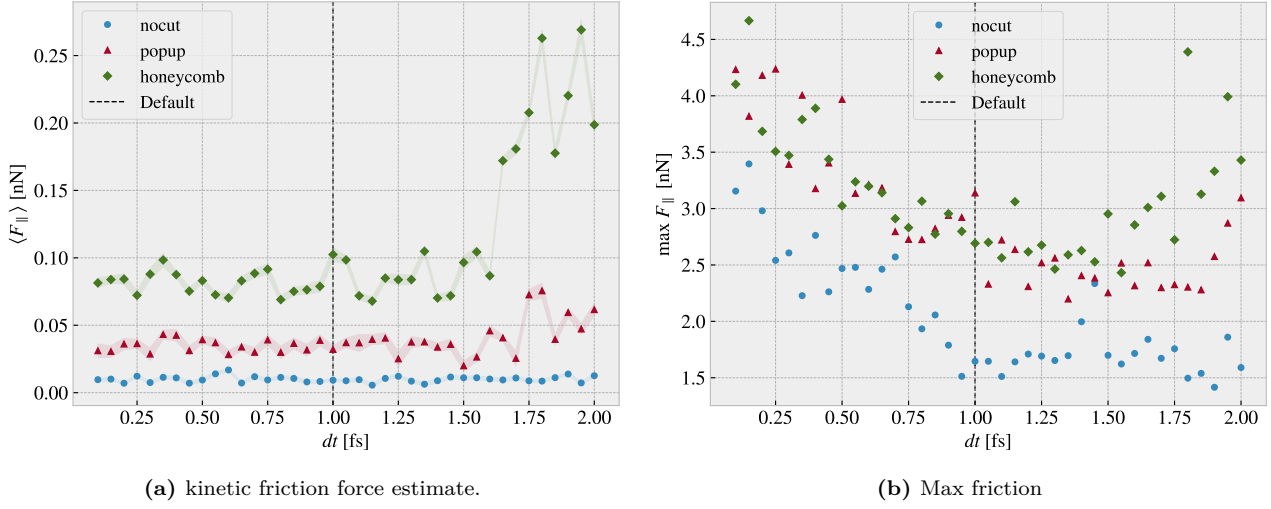


Figure 2.14: Timestep

Quick thoughts:

- Temperature: We do clearly not see the  $1/T$  temperature decrease. The non-cut sheet seems to showcase a linear relationship which is also somewhat present for the honeycomb which matches some of the findings in other MD simulations. For the popup we do see a local decrease at low temperatures which flip at around the default  $T = 300$  K temperature. The max friction peaks seem to increase with temperature as well indicating that the peaks might be associated with thermal fluctuations rather than actual stick-slip behaviour. This supports the finding that the static friction response is not significantly present in these simulations.
- Velocity: Considering the non-cut sheet first the velocity dependency is seemingly linear which deviates from the expected logarithmic trend. For the cutted configurations we find some peaks which might indicate the presence of resonance frequencies. The cutted sheet might be closer to a logarithmic trend, but this is not spot on either. The max friction seems to decrease slightly with small velocities and then stay rather constant. This can probably be explained by the reduced time to stick between stick slip.
- Spring constant: On all three configurations the kinetic friction decreases with an increasing spring constant. The best explanations might be due to the lack of freedom to “get stuck” in incommensurable configurations. We also notice that the friction varies a lot at lower spring constants supporting the choice of having a stiff spring for stability reasons. Especially the non-cut sheet peaks at  $K = 40$  N/m. The max friction seem to be constant with  $K$ .
- $dt$ : The kinetic friction is relatively stable around the default choice of  $dt = 1$  fs. However, the fluctuations with respect to  $dt$  is more significant for popup pattern and even more for the honeycomb pattern. This indicates that the more complex kinetics of the simulation is more sensitive to the timestep. We might interpret this information as an additional measure of uncertainty. The maximum friction decreases with increasing timestep which can be asserted a statistical interpretation: Higher peaks will be captured by the high resolution of a low  $dt$  and vice versa. The high max values towards the point of  $dt = 2$  fs is most likely due to the approach of instability in the simulation as seen more clearly for the kinetic friction evaluation.

## 2.6 Normal force and stretch dependencies

Till this point we have only changed variables one by one to investigate single dependencies. We now advance the study to a simultaneous variation of stretch and normal force.

Explain how the stretch is uniformly sampled within equally divided intervals and the normal force is actually uniformly sampled in a given range. Argue that the first might be approximately uniformly distributed for large numbers.

Talk about rupture test also. Maybe in the theory/method section under numerical procedure: Before simulating a rupture test is perform to determine under what stretch the sheet ruptures. This is a slightly higher threshold than when applied normal load and sliding along the substrate.

### 2.6.1 Pressure reference for normal load domain

In order to relate the magnitude of the normal force in our friction measurement we will use the pressure as a reference. We will use the pressure underneath a stiletto shoe as a worst case for human pressure execution underneath the shoes. From (source 1) it is reported that the diameter of a stiletto heeled shoe can be less than 1 cm. Hence a 80 kg man<sup>2</sup> standing on one stiletto heel (with all the weight on the heel) will result in a pressure

$$P = \frac{F}{A} = \frac{mg}{r^2\pi} = \frac{80 \text{ kg} \cdot 9.8 \frac{\text{m}}{\text{s}^2}}{(\frac{1 \times 10^{-2} \text{ m}}{2})^2\pi} = 9.98 \text{ MPa}$$

While this is in itself a spectacular realization that is often used in introductory physics courses (source 2) to demonstrate the rather extreme pressure under a stiletto heel (greater than the foot of an elephant) (how many Atmos?) this serves as a reasonable upperbound for human executed pressure. With a full sheet area of  $\sim 21 \times 10^3 \text{ \AA}^2$  we can achieve a similar pressure of  $\sim 10 \text{ MPa}$  with a normal force of

$$F_N = 10 \text{ MPa} \cdot 21 \times 10^{-17} \text{ m}^2 = 2.10 \text{ nN}$$

Of course this pressure might be insufficient for various industrial purposes, but with no specific procedure in mind this serves as a decent reference point. Notice that if we consider a human foot with area  $113 \text{ cm}^2$  the pressure drops to a mere 70 kPa corresponding to  $\sim 0.01 \text{ nN}$ .

### 2.6.2 Contact area

??

We reproduce the contact area investigation of Fig. 2.10 with the modification that the contact count is measured as an average of the latter 50% of the sliding simulation at a non-zero applied normal load. The results are shown in Fig. 2.15 with 30 attempted (some rupture) stretch (pseudo) uniformly distributed stretch between 0 and the rupture point and 3 uniform distributed normal loads in the interval [0.1, 10] nN.

---

<sup>2</sup>Yes, a man can certainly wear stiletto heels.

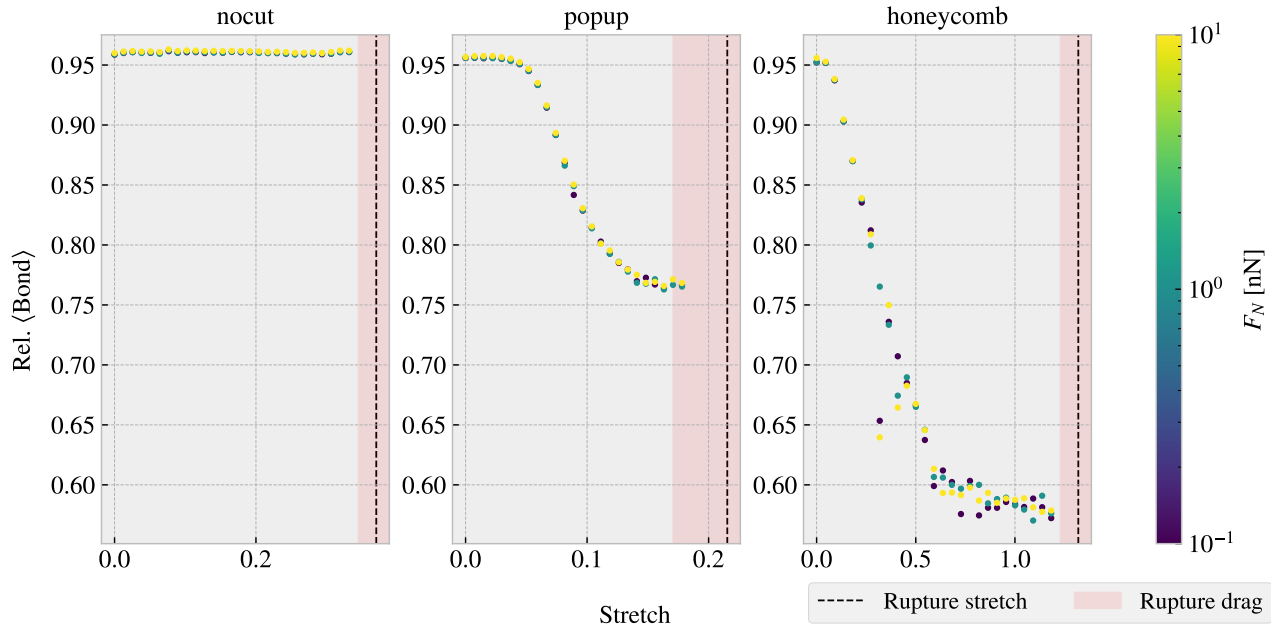


**Figure 2.15:** Average relative amount of bonds between the sheet and the substrate defined by the cut-off distance of 4 Å. The average is taken over the latter half of the sliding phase. The red shade denotes the stretch range where ruptures accrue at certain normal loads under sliding while the black-dotted line represent the rupture point due to stretching (rupture test)

From Fig. 2.10 we observe a significant decrease in the contact due to stretching of the cut configurations in contrast to the non-cut which stays roughly constant. This is reminiscent of the non-sliding stretch vs. contact curve shown in Fig. 2.10. Given these results, theoretically one would expect the kinetic friction to decrease with stretch for the cut configurations.

### 2.6.3 Stretch

We make a similar analysis as done in the previous section ?? with the substitution of friction force instead of contact (The data is taken from the same simulations runs). The kinetic friction force (put uncertainty here even though that it is quite low?) and the max friction is shown in Fig. 2.16a and Fig. 2.16 respectively.

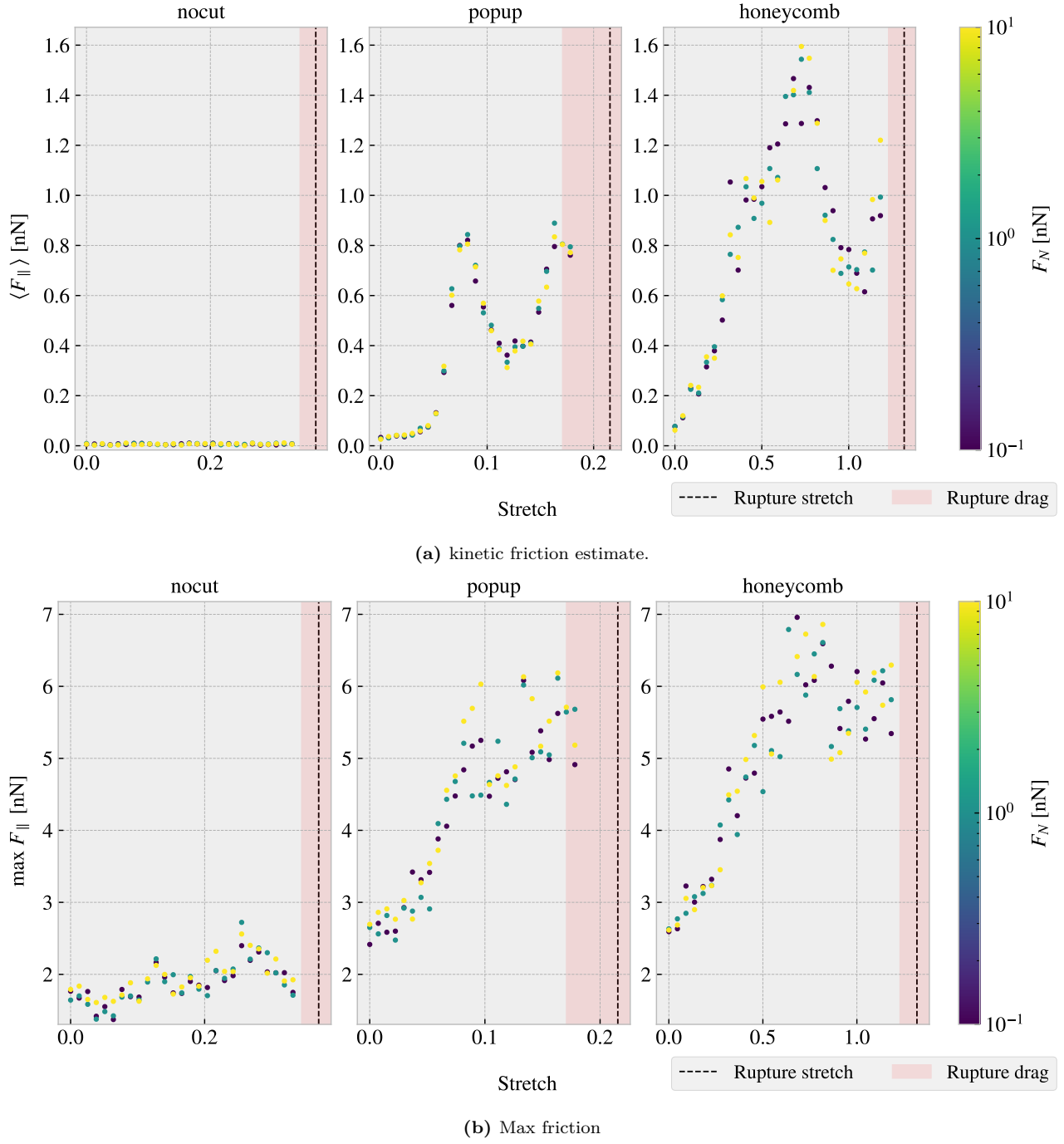


Figure 2.16: CAPTION

From Fig. 2.16a we find to our surprise that the kinetic friction increase with stretch for the cut configurations despite a simultaneous decrease in contact area as shown in figure Fig. 2.15. This suggests that the amount of chemical bonding atoms is not the dominant mechanism for the friction of this system. Instead, we might point to a mechanism more mechanical of nature associated to phonon excitations. When the cut sheet is stretched the stress (show stress maps somewhere or not necessary?) might induce a certain distribution and magnitude of point pressures to favor energy dissipation. Nonetheless, the results showcase a strong coupling between stretch and friction force, also for the max friction force, which is beyond the expectations at this stage of the study. The non-cut configuration does not show significant dependency on the stretch which reveal that this effect is only present when combining cut and stretch and not purely by stretching the sheet.

By considering the increase in kinetic friction towards the first peak we get a relative friction increase and increase vs. stretch ratios as described in Table 2.2. While the honeycomb force increase towards the first peak is approximately linear the popup exhibits seemingly exponential growth which yield a slope on the order  $\sim 30$  nN.

**Table 2.2:** (stretch, kinetic friction) coordinates from Fig. 2.16a at start and the first peak respectively used to approximate the relative increase in friction force and the ratio for friction increase vs. stretch for sait range. In practice the latter ratio denotes the slope of a forced linear trend.

Configuration	Start	First peak	Relative increase	Friction force vs. stretch ratio [nN]
Popup	$\sim (0, 0.03)$	$\sim (0.082, 0.83)$	27.7	9.76
Honeycomb	$\sim (0, 0.07)$	$\sim (0.728, 1.57)$	22.4	2.06

Additionally, we notice that both the popup and honeycomb also exhibits stretch ranges where the kinetic friction force decrease with increasing stretch. Qualitatively we assign the slope to be on the same order of magnitude as those towards the first peak. This is useful for the prospect of taking advantage of this phenomena as we can essentially achieve both higher and lower friction for increasing stretch for different starting points.

#### 2.6.4 Normal force

Main take away from this section should be that the normal force does not really change the friction much; The friction coefficient is extremely low, but I'm not sure how well the linear fits are (whether they are linear or sublinear). Not sure if I should do a linearly increasing normal force for better linear plots?

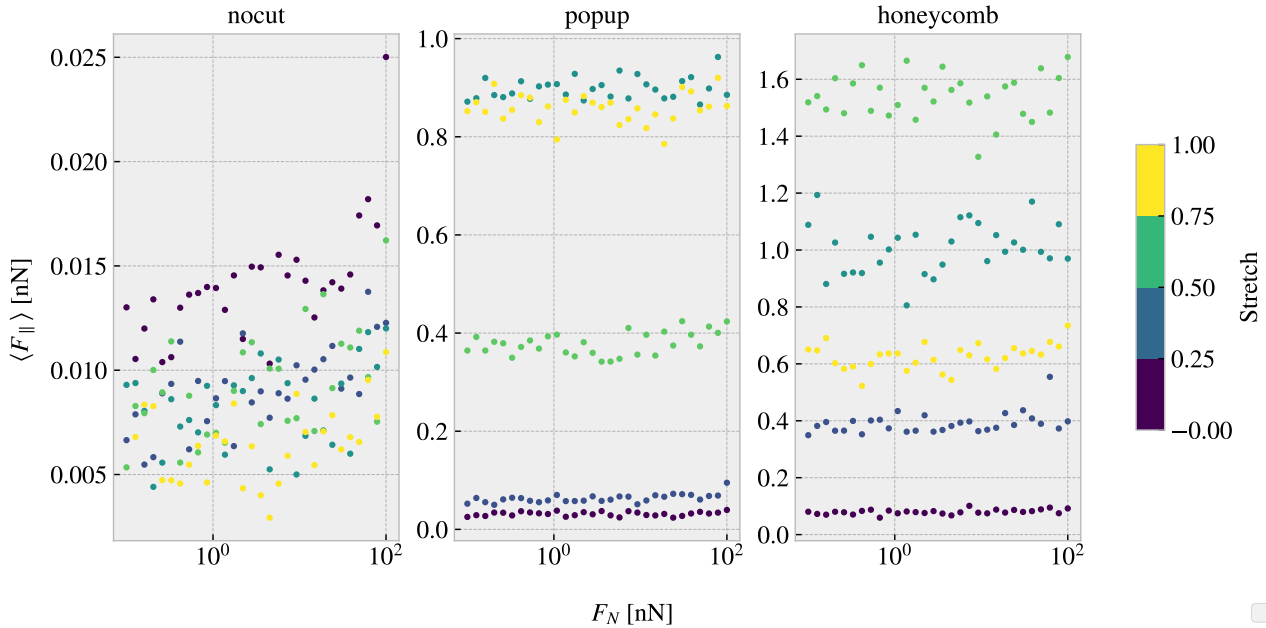


**Figure 2.17:** ...

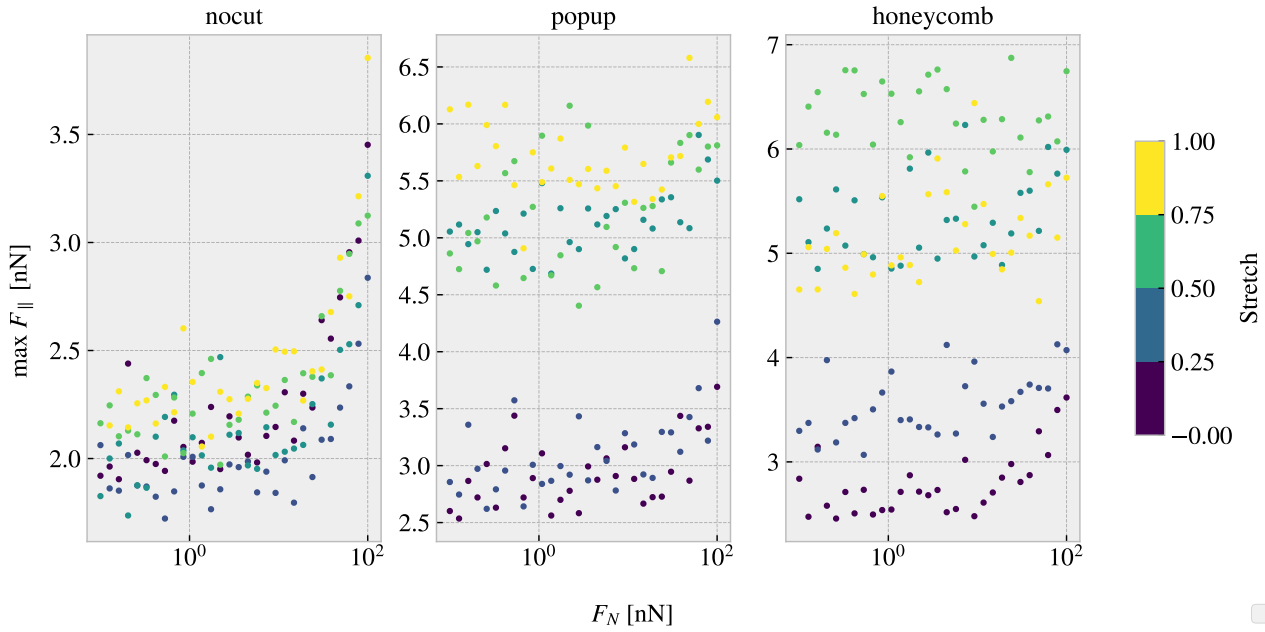


**Figure 2.18:** Colorbar is only fitted for the right plot (honeycomb)... this should be fixed. Should I have run a linear distribution of FN so I could plot it linear here also...?

**Table 2.3:** Mean friction coeff

nocut	$0.00009 \pm 1 \times 10^{-5}$	$0.00005 \pm 1 \times 10^{-5}$	$0.00004 \pm 1 \times 10^{-5}$	$0.00005 \pm 2 \times 10^{-5}$	
popup	$0.00005 \pm 3 \times 10^{-5}$	$0.00024 \pm 5 \times 10^{-5}$	$0.0002 \pm 2 \times 10^{-4}$	$0.0005 \pm 1 \times 10^{-4}$	$0.0003 \pm 2 \times 10^{-4}$
honeycomb	$0.00013 \pm 6 \times 10^{-5}$	$0.0006 \pm 3 \times 10^{-4}$	$0.0004 \pm 6 \times 10^{-4}$	$0.0007 \pm 6 \times 10^{-4}$	$0.0009 \pm 3 \times 10^{-4}$

**Table 2.4:** Max friciton coeff

nocut	$0.0139 \pm 9 \times 10^{-4}$	$0.0083 \pm 7 \times 10^{-4}$	$0.010 \pm 1 \times 10^{-3}$	$0.0105 \pm 9 \times 10^{-4}$	
popup	$0.007 \pm 2 \times 10^{-3}$	$0.010 \pm 2 \times 10^{-3}$	$0.007 \pm 2 \times 10^{-3}$	$0.009 \pm 3 \times 10^{-3}$	$0.006 \pm 2 \times 10^{-3}$
honeycomb	$0.010 \pm 1 \times 10^{-3}$	$0.007 \pm 2 \times 10^{-3}$	$0.007 \pm 3 \times 10^{-3}$	$0.000 \pm 3 \times 10^{-3}$	$0.004 \pm 3 \times 10^{-3}$

One theory for the low friction coefficient might dependent on the fact that the normal force is only applied on the pull blocks. Especially with the cutted sheet the tension drops such that the effecive normal force on the inner sheet is not changing very much. By this theory the friction force vs. normal force on the pull blocks should look a bit more like expected and we might make some plots of thoose to check

When looking at the graphs for the PB the max friction is visually textbook linear, while the mean friction is a bit more linear but also with negativ coefficients...

## 2.7 Computational cost

Talk about the computatational cost of different choices. How does computation time scale with drag speed,  $dt$  and maybe  $T$  and  $K$  as well. One could also mention scaling with system size.

Show how the number of cores per simulation scale to argue that running on just one core (maybe 4) is smart for the next step of many simulations.

Mention the trouble with GPU to show that this was considered, and in fact this was the reason for choosing the Tersoff potential over the AIREBO which is perhaps more common these days...



# Appendices



# Appendix A

## A.1 Sheet stretch

Some information about the following figures. We used a slower stretch speed of  $0.001 \text{ ps}^{-1} = 0.1\%/\text{ps}$  for these simulations to get more clean figures although did this not make any noticeable changes to the plots of the contact area. We used  $T = 5 \text{ K}$  for the vacuum simulation in (in order to reduce vibration) and  $T = 300 \text{ K}$  for the contact simulation.

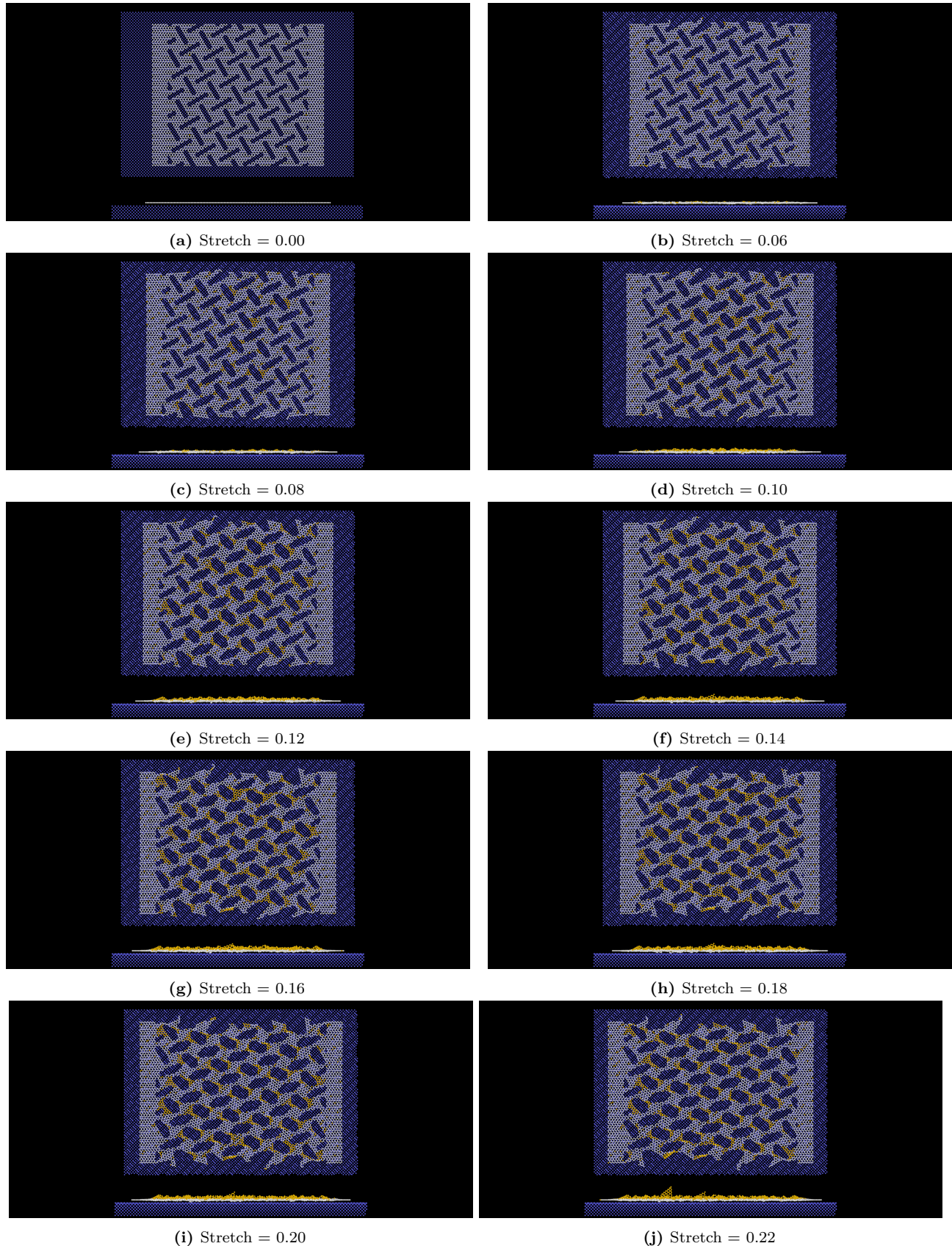


**Figure 19:** Stretch of Tetrahedron (7, 5, 1) against substrate. Top part of each frame (a)-(j) shows a top-down view with axis (y, x), and the bottom part shows a side-view with axis (y, z). White colored atoms indicate graphene sheet carbon atoms in contact with the substrate while the yellow colored atoms are not in contact.

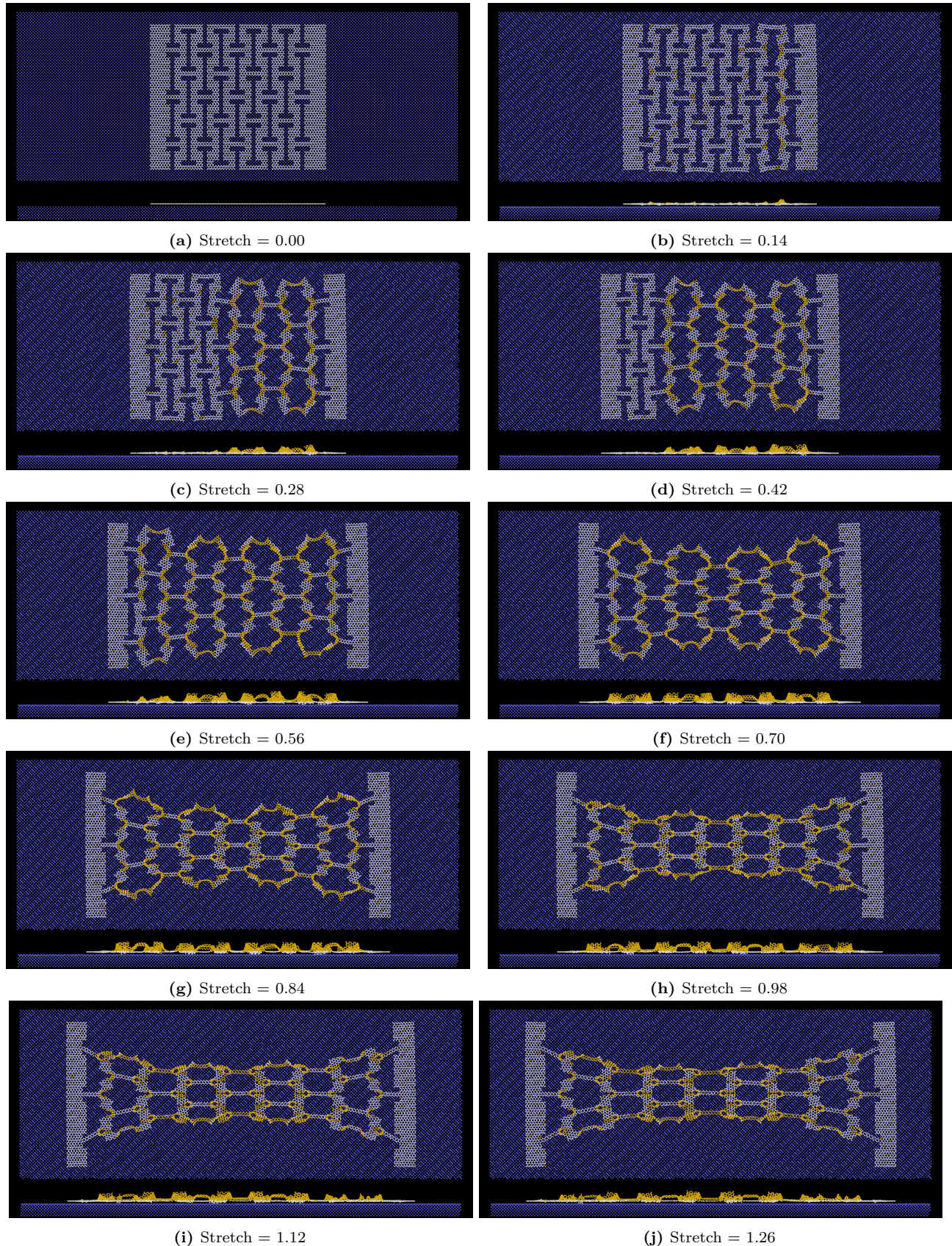


**Figure 20:** Stretch of Honeycomb (2, 2, 5, 1) pattern against substrate. Top part of each frame (a)-(j) shows a top-down view with axis (y, x), and the bottom part shows a side-view with axis (y, z). White colored atoms indicate graphene sheet carbon atoms in contact with the substrate while the yellow colored atoms are not in contact.



# Appendix B



# Appendix C



# Bibliography

- <sup>1</sup>E. Gnecco and E. Meyer, *Elements of friction theory and nanotribology* (Cambridge University Press, 2015).
- <sup>2</sup>Bhusnur, “Introduction”, in *Introduction to tribology* (John Wiley & Sons, Ltd, 2013) Chap. 1, 1–?
- <sup>3</sup>H.-J. Kim and D.-E. Kim, “Nano-scale friction: a review”, *International Journal of Precision Engineering and Manufacturing* **10**, 141–151 (2009).
- <sup>4</sup>K. Holmberg and A. Erdemir, “Influence of tribology on global energy consumption, costs and emissions”, *Friction* **5**, 263–284 (2017).
- <sup>5</sup>B. Bhushan, “Gecko feet: natural hairy attachment systems for smart adhesion – mechanism, modeling and development of bio-inspired materials”, in *Nanotribology and nanomechanics: an introduction* (Springer Berlin Heidelberg, Berlin, Heidelberg, 2008), pp. 1073–1134.
- <sup>6</sup>P. Z. Hanakata, E. D. Cubuk, D. K. Campbell, and H. S. Park, “Accelerated search and design of stretchable graphene kirigami using machine learning”, *Phys. Rev. Lett.* **121**, 255304 (2018).
- <sup>7</sup>P. Z. Hanakata, E. D. Cubuk, D. K. Campbell, and H. S. Park, “Forward and inverse design of kirigami via supervised autoencoder”, *Phys. Rev. Res.* **2**, 042006 (2020).
- <sup>8</sup>L.-K. Wan, Y.-X. Xue, J.-W. Jiang, and H. S. Park, “Machine learning accelerated search of the strongest graphene/h-bn interface with designed fracture properties”, *Journal of Applied Physics* **133**, 024302 (2023).
- <sup>9</sup>Y. Mao, Q. He, and X. Zhao, “Designing complex architectured materials with generative adversarial networks”, *Science Advances* **6**, eaaz4169 (2020).
- <sup>10</sup>Z. Yang, C.-H. Yu, and M. J. Buehler, “Deep learning model to predict complex stress and strain fields in hierarchical composites”, *Science Advances* **7**, eabd7416 (2021).
- <sup>11</sup>A. E. Forte, P. Z. Hanakata, L. Jin, E. Zari, A. Zareei, M. C. Fernandes, L. Sumner, J. Alvarez, and K. Bertoldi, “Inverse design of inflatable soft membranes through machine learning”, *Advanced Functional Materials* **32**, 2111610 (2022).
- <sup>12</sup>S. Chen, J. Chen, X. Zhang, Z.-Y. Li, and J. Li, “Kirigami/origami: unfolding the new regime of advanced 3D microfabrication/nanofabrication with “folding””, *Light: Science & Applications* **9**, 75 (2020).
- <sup>13</sup>Z. Deng, A. Smolyanitsky, Q. Li, X.-Q. Feng, and R. J. Cannara, “Adhesion-dependent negative friction coefficient on chemically modified graphite at the nanoscale”, *Nature Materials* **11**, 1032–1037 (2012).
- <sup>14</sup>R. W. Liefferink, B. Weber, C. Coulais, and D. Bonn, “Geometric control of sliding friction”, *Extreme Mechanics Letters* **49**, 101475 (2021).
- <sup>15</sup>P. Zhu and R. Li, “Study of nanoscale friction behaviors of graphene on gold substrates using molecular dynamics”, *Nanoscale Research Letters* **13**, 34 (2018).
- <sup>16</sup>S. Li, Q. Li, R. W. Carpick, P. Gumbsch, X. Z. Liu, X. Ding, J. Sun, and J. Li, “The evolving quality of frictional contact with graphene”, *Nature* **539**, Number: 7630, 541–545 (2016).